## PAPER

Check for updates

# Construction of pH/reduction dual responsive MSN-HAgel containing HApt for tumor targeting carriers†

Yehong Liu, Miaoxin Chen, Gaoyang Li, Shouhong Xu [ID] * and Honglai Liu

In this study, a pH/reduction dual responsive carrier containing 42nt-nucleic acid HApt based on mesoporous silica nanoparticles (MSNs) was designed. Two kinds of low molecular weight oligomeric hyaluronic acid (HA) were used to graft onto MSN for better drug encapsulation. Crosslinked MSN-HA$_{3000}$gel and MSN-HA$_{11000}$gel were prepared by crosslinking the HA chain through the sulfhydrylization of the carboxyl group on the HA side chain. An appropriate amount of sulfhydryl nucleic acid (HApt-SH) was added during the crosslinking reaction, which realized the targeting ability and apoptosis function to cancer cells overexpressing the HER2 receptor. Crosslinked HA had a good effect on decreasing the side effect of DOX that the drug leakage was less than 20% under a normal body environment. However, it could realize rapid and efficient drug release in a tumor environment. As to the release of HApt, it exhibited a good response to GSH. The cytotoxicity test showed that HApt contained in HAgel had a great targeting effect and significant cytotoxicity to SKBR3 cells. As a whole, this MSN-HAgel enabled the combination of gene therapy and chemotherapy, showing the synergistic effect of "1 + 1 > 2", providing a novel idea for cancer treatments.

## 1. Introduction

Due to factors such as environmental pollution and population aging, cancers, particularly lung cancers,[1] have become one of the major diseases threatening human health.[2,3] Chemotherapy, as one of the three main therapies, is limited by toxic and side effects to normal cells and drug resistance of cancer cells[4–6] because of the low concentration of effective drugs in the tumor area.[7] Therefore, effectively improving the targeting of anti-tumor drugs to tumor tissues and controlling the release of drugs have become the focus of contemporary medical research.[8]

Smart drug-loaded nanocarriers, also called stimulus-responsive or environment-responsive drug-loaded nano-carriers, have attracted widespread attention and research.[9,10] According to different external environmental stimulus signals, such as temperature, pH, solvent, ion, reduction, ultrasound and other responses, they can be divided into different types.[11–13] Smart drug-loaded nanocarriers have numerous advantages: small carrier particle size, large specific surface area, increasing the solubility of hydrophobic or poorly soluble drugs,[14,15] increasing the cell uptake rate of drugs, prolonging

the cycle of drug circulation in the body, facilitating the drug concentration at tumor sites, *etc.*[16,17]

Mesoporous silica nanoparticles (MSNs) are widely used as nanocarriers due to their advantages of good biocompatibility, large specific surface area, orderly and adjustable pore size, and easy modification of surface.[18–20] As early as in 2003, Lin *et al.*[21] used cadmium sulfide (CdS) quantum dots as a plugging material for mesoporous materials, and used mesoporous silica for the first time to study the release of environmentally stimulating carriers. Since then, a series of "gates" for mesoporous silica drug delivery systems have been constructed,[22] such as inorganic nanoparticles,[23] polymers,[24] and biological macro-molecules.[25] Hyaluronic acid (HA) is a viscous polysaccharide with a unique linear macromolecular structure composed of disaccharide units repeatedly connected by glucuronic acid and *N*-acetylglucosamine,[26,27] which is widely distributed in the extracellular matrix of connective tissues of humans and animals.[28,29] It is widely used in the medical field and cosmetics because of its high viscoelasticity, permeability, excellent biocompatibility and degradability. Its receptor CD44 is highly expressed in numerous tumor cells such as MDA-MB-231 cells.[30,31] Targeted drug delivery can be achieved by modifying the HA on the drug-carrying system and the defect of silica particles that are prone to agglomeration can also be solved. The electrostatic interactions and hydrogen bonds between HA chains at different pHs also make HA-modified silica nano-particles responsive to pH.[32,33] Ghosh *et al.*[34] prepared curcumin-loaded hyaluronic acid functionalized mesoporous

*State Key Laboratory of Chemical Engineering and School of Chemistry & Molecular Engineering, East China University of Science and Technology, Shanghai, 200237, P.R. China. E-mail: xushouhong@ecust.edu.cn*

† Electronic supplementary information (ESI) available. See https://doi.org/10.1039/d2ra02290g

silica nanoparticles. Zhang et al.[35] used disulfide bonds to fix HA on the surface of MSNs as a "guard" to encapsulate DOX.

Oligonucleotides are also widely used in cancer treatment in the recent years.[36–38] The encapsulation of nucleotide molecules by smart drug carriers can protect them from being cleared by the human immune system and achieve their enriching in the tumor area. Human epidermal growth factor receptor (HER2) is highly expressed on various cancer cells.[39] Reducing the expression of HER2 receptor on the surface of cancer cells can change its downstream signal channels and lead to cell cycle arrest and cell apoptosis. At present, a 42nt nucleic acid molecule HApt has been reported to bind to the HER2 receptor and transfer it from the cell membrane to the intracellular lysosome for enzymolysis.[40,41] The reduction of HER2 protein on the cell membrane surface induced the death of HER2-overexpressed N87 gastric and SKBR3 breast cancer cells.[42] In our lab, Yingxing Shen[43] prepared pH-sensitive polymer micelles to carry nucleic acid molecules into cancer cells.

The pH/redox controlled release system in this paper was mainly designed according to the different redox and pH environments of the internal and external environment of tumor cells. MSNs were used as a core and then HA was grafted onto the surface. HAgel layer formed due to the crosslinking between sulfhydryl-modified HA and HApt-HS, and oligonucleotide molecules were introduced at the same time. When the drug-loaded nanocarrier reached the tumor site, i.e., high concentration of GSH and acidic conditions, the disulfide bond was ruptured and electrostatic attraction between the HA chain and DOX disappeared, which led to efficient release of DOX. At the same time, the recognition of HApt and HER2 receptor could target lysosomes and lead to degradation of HERE protein, which induced apoptosis.[42] This drug delivery system (DDS) designed here was expected to realize the synergistic effect of gene therapy and drug therapy, which is represented in Scheme 1.

# 2. Experimental section

## 2.1. Materials and reagents

Cetyltrimethylammonium bromide (CTAB, 99%), disodium hydrogen phosphate (Na$_2$HPO4, AR), and sodium dihydrogen phosphate (NaH$_2$PO$_4$, AR) were purchased from Shanghai Titan Company. Tetraethyl orthosilicate (TEOS, 99%) was purchased from Saen Chemical Technology (Shanghai) Company. (3-Aminopropyl) triethoxysilane (KH550, 98%) was purchased from Shanghai Xushuo Biotechnology Co., Ltd. N-hydroxysulfonylsuccinimide (NHS, 98%), 1-ethyl-(3-methylaminopropyl) carbodiimide hydrochloride (EDC·HCl 99%), glutathione (reduced type, GSH, 98%), and cysteamine hydrochloride (Cys·HCl, 98%) were purchased from Shanghai Macklin Biochemical Company. Tris(2-chloroethyl) phosphate (TCEP) was purchased from Shanghai Aladdin Biochemical Technology Co., Ltd. Doxorubicin hydrochloride (DOX·HCl, 98%) was purchased from J&K. Sodium cyanoborohydride (NaBH$_3$CN, 95%) was purchased from Shanghai Jiuding Chemical Technology Company. Sodium hyaluronate (low-molecular-weight NaHA, $M_W$: 3000, 11 000) was purchased from Shanghai Yuanye Biological Company. 42nt-oligomeric acid (HApt-SH, 5′-SH-GCAGCGGTGTGGGG/GCAGCGGTGTGGGG/GCAGCGGTGTGGGG-3′, AR) and Texas Red-42nt-oligomeric acid (Texas Red-HApt-SH, AR) were purchased from Sangon Biotech (Shanghai) Company. Ultrapure water (H$_2$O, 18.2 MΩ) and high purity nitrogen (N$_2$, high purity) were used throughout the study.

## 2.2. Synthesis

The main synthetic route is listed in Scheme 2.

**2.2.1 Synthesis of MSN-NH$_2$.** MSN was synthesized by the hydrolysis method. In brief, CTAB was dissolved in pure water and 2 M NaOH was dropped. Then, TEOS was added dropwise and reacted for 2 h. After sedimentation, centrifugation and
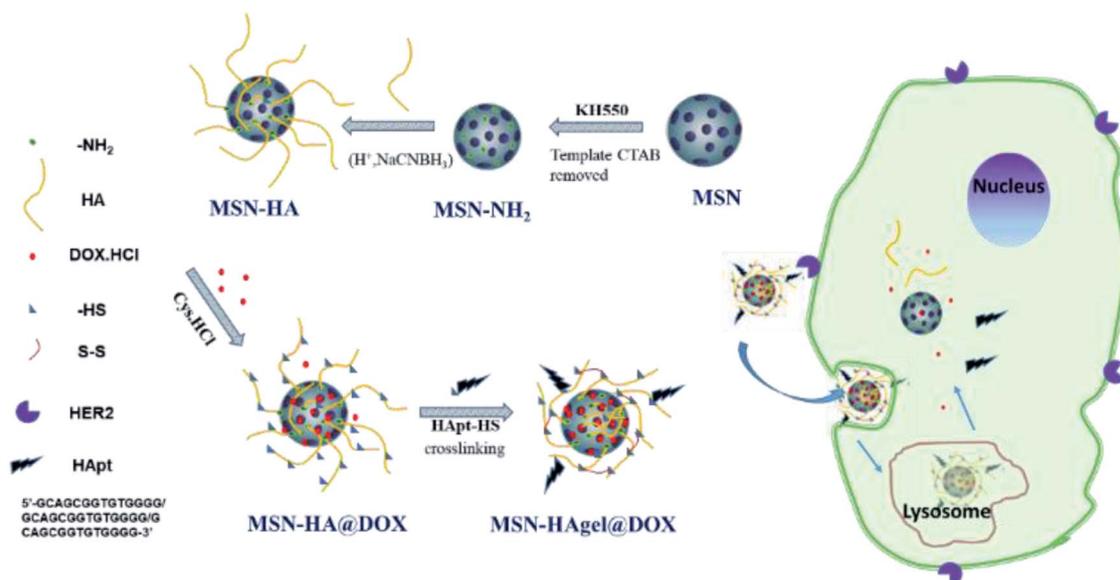


**Scheme 1** Schematic representation for the construction of MSN-HAgel@DOX and the mechanism of tumor-targeted combined therapy.
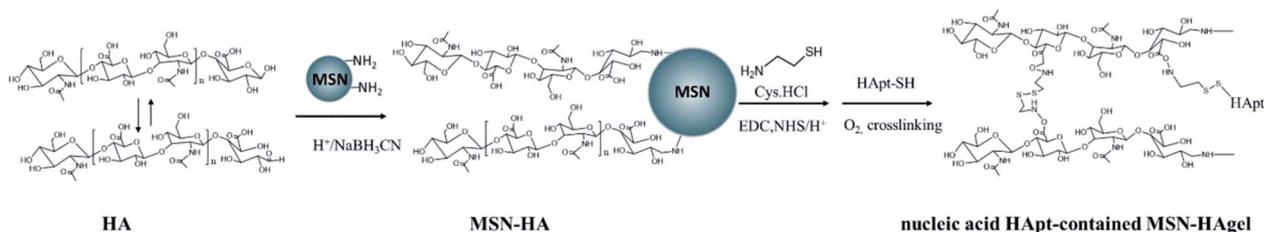
**Scheme 2** Main synthetic route of MSN–HAgel.

washing, the MSN was obtained. A silane coupling agent KH550 was added in MSN and the reaction was refluxed at 110 °C for 12 h. The methanol and concentrated HCl were added at 65 °C for 12 h to remove the template CTAB. Finally, surface-aminated mesoporous silica (MSN-NH$_2$) was obtained after centrifugation and washing with methanol and water alternately.

**2.2.2 Preparation of MSN-HA.** MSN-HA was prepared by the reductive amination reaction between the amino group on MSN and the dynamic aldehyde group at the end of HA (MW: 3000, 11 000 Da). The products were referred to as MSN-HA$_{3000}$ and MSN-HA$_{11000}$ according to the molar weight of HA. To prepare MSN-HA$_{3000}$, sodium hyaluronate (NaHA) was dissolved in pure water and then placed in a dialysis bag (800 Da). After dialysis with 2 M HCl for 5 h and ultrapure water for 3 h, the HA powder was obtained by freeze-drying. MSN-NH$_2$ was dispersed in PBS and HA (Mw: 3000 Da, 0.776 g, 0.26 mmol) was added, and then 2 M HCl was added until the pH was adjusted to about 4.5. Then sodium cyanoborohydride (NaBH$_3$CN, 46.1 mg, 1.032 mol) was added in N$_2$ and then reacted at 60 °C for 48 h. After centrifugation and washing with PBS, white solid MSN-HA$_{3000}$ was obtained by freeze-drying.

**2.2.3 Preparation of MSN-HA@DOX and MSN-HAgel@-DOX.** Firstly, DOX was added into MSN-HA solution and stirred for 24 hours under dark for preparing MSN-HA@DOX. The unloaded DOX was washed away with PBS (pH 7.4) and the UV absorption value of the supernatant was detected. The drug encapsulation efficiency (DEE) and drug-loading content (DLC) were obtained by detecting the UV absorption value at 485 nm with a UV-vis spectrophotometer (UV-2450, Shimadzu, Japan). The values of DEE and DLC were calculated using the following equations:

$$DEE(\%) = \frac{\text{Weight of the drug in the carriers (mg)}}{\text{Weight of the drug in feed (mg)}} \times 100 \quad (1)$$

$$DLC (\%) = \frac{\text{Weight of the drug in the carriers (mg)}}{\text{Weight of the carriers (mg)}} \times 100 \quad (2)$$

Then, the carboxyl group on the HA side chain was modified by the –SH group for the further crosslink reaction to form a S–S bond. In detail, MSN-HA@DOX was dispersed in PBS and *N*-hydroxysulfonylsuccinimide (NHS, 4.5 mg, 0.042 mmol) and 1-ethyl-(3-methylaminopropyl) carbodiimide hydrochloride (EDC·HCl, 11.9 mg, 0.044 mmol) were added and reacted for 6 h. Subsequently, cysteine hydrochloride (Cys·HCl, 7.1 mg,

0.041 mmol) and 3 nmol HApt-HS were added and stirred for 12 h. Finally, the system was exposed to air and reacted for 24 h for HA gel formation. The product carried HApt on the HA gel layer, which was denoted as MSN-HAgel@DOX.

### 2.3. Characterization

Fourier transform infrared spectroscopy (FT-IR), thermogravimetric analysis (TGA), Brunner–Emmett–Teller nitrogen adsorption/desorption (BET), transmission electron microscopy (TEM) and dynamic light scattering (DLS; Zetasizer Nano-ZS, Malvern, UK) were performed to confirm the successful synthesis and the composition.

**2.3.1 Physicochemical properties of the carriers.** DLS was mainly used to analyze the properties of nanocarriers at different pHs. MSN-HA and MSN-HAgel ($c = 0.1$ mg mL$^{-1}$) containing PBS buffer solution with different pHs were prepared to measure their sizes and potentials.

*In vitro* drug release of MSN-HAgel. The release of the encapsulated drug and the grafted HApt molecules was investigated separately. For the needs of detection, fluorescently labeled HApt molecules were used in the synthesis of the MSN-HAgel for HApt release.

*In vitro* drug release of DOX: 2 mg MSN-HAgel@DOX was added into centrifuge tubes containing 15 mL different PBS (pH 7.4, pH 7.4 + 10 mM GSH, pH 5.0, pH 5.0 + 10 mM GSH). The centrifuge tube was numbered and placed in a constant temperature shaking box at 37 °C. During a specific time interval, 2 mL of the supernatant was taken for fluorescence intensity analysis and then the supernatant was poured back. The DOX fluorescence intensity at 550 nm of the supernatant was detected with a fluorescence spectrometer (F-4500, Hitachi, Japan). The cumulative release ratio was calculated by the following equation:

$$\text{Cumulative release } (\%) = \frac{A_t}{A_0} \times 100 \quad (3)$$

where $A_t$ represents the fluorescence intensity of DOX at time $t$, and $A_0$ represents the amount of encapsulated DOX. $A_0$ was obtained by subtracting the unloaded DOX from DOX in feed.

*In vitro* drug release of Texas Red-HApt: 2 mg MSN-HAgel was taken into a centrifuge tube containing 25 mL different PBS (pH 7.4, pH 7.4 + 10 mM GSH, pH 5.0, pH 5.0 + 10 mM GSH) and then placed in a constant temperature shaking box at 37 °C. The fluorescence intensity at 610 nm of the supernatant was detected with a fluorescence spectrometer. The cumulative release ratio was also calculated by eqn (3).

Cell culture. The hepatoma cell HepG2 and the breast cancer cell SKBR3 overexpressing the HER2 receptor were selected for biocompatibility and cytotoxicity experiments. Both cells were purchased from ATCC (USA). Both types of cells were recovered into a Petri dish and corresponding medium (DMEM for HepG2 cells and McCoy's 5A medium for SKBR3 cells; containing 1% artemisinin G/streptomycin sulfate and 10% fetal bovine serum) was added subsequently. Then they were put into a cell incubator for incubation and passage (37 °C, 5% $CO_2$) to enhance cell viability.

Biocompatibility and cytotoxicity assays. A certain amount of MSN-HAgel and MSN-HAgel@DOX with different concentrations were added to the 96-well plate with cells, and co-incubated for 4 h for cell transfection. Then, the medium was changed to serum-free medium and incubated for 24 h. Subsequently, the supernatant medium was removed and serum-free medium containing 10% CCK-8 stain was added. The absorption of each well plate at 450 nm was detected with a microplate reader to quantitatively detect the cell viability.

## 3. Results and discussion

### 3.1. The synthesis of MSN-HAgel

In this study, two molar weights of HA were selected for modifying MSN. In the results and discussion section, it was mainly showed the results of products synthesised by HA with its molar weight 3000. Data were presented as mean ± standard deviation (s.d.) and were analyzed using two-way analysis of variance (ANOVA).

IR spectra graphs of MSN, MSN-NH₂, MSN-HA and MSN-HAgel and TGA curve of MSN, MSN-NH₂ and MSN-HA are shown in Fig. S1†. In short, the characteristic absorption peak appeared at 1625.6 cm⁻¹ of C=O on MSN-HA curve and 1655 cm⁻¹ of amide I bond on MSN-HAgel. Moreover, TGA showed that the grafting mass rate of amino groups was about 7.14% and the grafting amount of $HA_{3000}$ and $HA_{11000}$ was about 10.72% and 19.1%.

The BET nitrogen adsorption/desorption isotherms and BJH pore size distribution of MSN, MSN-HA and MSN-HAgel@DOX are shown in Fig. S2.† The mesoporous structure of MSN showed an orderly typical type IV isotherm. With the modification of the MSN surface, its BET surface area ($S_{BET}$) and pore volume ($V_P$) were reduced (Table 1); $S_{BET}$ decreased from 1118 to 48 m² g⁻¹, while $V_P$ decreased from 0.73 cm³ g⁻¹ to 0.09 cm³ g⁻¹. However, it's worth noting that the BJH pore size ($D_{BJH}$) of
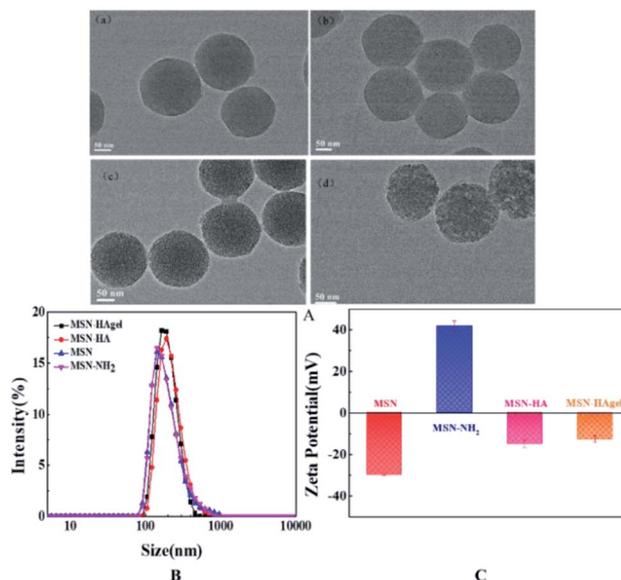


Fig. 1 TEM images (A) of (a) MSN, (b) MSN-NH₂, (c) MSN-HA₃₀₀₀, (d) MSN-HA₃₀₀₀gel; and their size distribution (B) and zeta potential values (C) ($c = 0.3$ mg mL⁻¹).

MSN-HA increased from 2.3 to 6.0 nm after HA was grafted and decreased to 0.1 nm after crosslinking. The reason for the rise was possibly due to the brush-like structure of the HA layer, which caused the pore size to increase. Then, after HA crosslinking, all the pores had been filled by gel so that the $S_{BET}$ reduced from 254 m² g⁻¹ to 48 m² g⁻¹ and both the $V_P$ and $D_{BJH}$ reduced to near zero, indicating that the HA gel layer could successfully block the pores.

TEM images, particle size distributions and zeta potential values of MSN, MSN-NH₂, MSN-HA and MSN-HAgel were measured under neutral conditions (Table S1† and Fig. 1). As shown in Fig. 1A(a), there were no significant differences between the aminated MSN and the MSN, but their zeta potential significantly reversed from −30 mV to +40 mV (Fig. 1C), which indicated the successful modification of the amino group. From Fig. 1 A(c) and Fig. 1B, it could be found that MSN-HA₃₀₀₀ kept the microsphere morphology with a rough surface structure and its diameters increased from 212.8 nm to 230.9 nm after HA was grafted (Table S1†), which indicated the successful grafting of HA. Moreover, zeta potential reversed again from +40 mV to −11 mV because of the large number of carboxyl groups on HA under neutral conditions. Furthermore,

Table 1   BET and BJH measurements for MSN before and after grafting with functional groups

| Samples | BET surface area, SBET (m² g⁻¹) | BET pore volume, Vp (cm³ g⁻¹) | Pore diameter, DBJH (nm) |
| --- | --- | --- | --- |
| MSN | 1118 | 0.73 | 2.6 |
| MSN-NH₂ | 760 | 0.44 | 2.3 |
| MSN-HA₃₀₀₀ | 254 | 0.38 | 6.0 |
| MSN-HA₃₀₀₀@DOX | 48 | 0.09 | 0.1 |
| MSN-HA₁₁₀₀₀ | 310 | 0.35 | 5.7 |
| MSN-HA₁₁₀₀₀gel@DOX | 30 | 0.07 | 0.1 |

after the crosslinking of the HA layer, the size slightly reduced from 230.9 nm to about 220 nm, and also their morphology changed accordingly. A subtle network structure of gel could be seen from the TEM image (Fig. 1A(d)).

### 3.2. Properties of the nanoparticles before and after crosslinking

**3.2.1 Response to pH.** The pH-responsive characteristics of MSN-HA$_{3000}$ (Fig. 2A) and MSN-HA$_{3000}$gel (Fig. 2B) were studied by their size and zeta potential under different pHs.

As shown in Fig. 2, their biggest difference was the trend of size change. The size of MSN-HA decreased with increasing pH; however, that of MSN-HAgel had an evident increase during pH 5–7. In a strong acid environment as shown in Fig. 2A, the particles showed very large size, indicating the state of aggregation. HA was neutrally charged due to the presence of –COOH, so MSN-HA aggregated and the brush-like structure collapsed so that the amino groups on the surface of MSN were exposed and accepted protons, resulting in an increased charge. Although there were electrostatic repulsions due to the positive charge, the hydrogen bond shall be stronger and induced the particles to assemble. However, as shown in Fig. 2B, the hydrogen bond was hidden by HA gel and MSN-HAgel could keep dispersion state. Next, when pH increased, MSN-HA charged negatively due to HA deprotonation, resulting in good dispersion due to electrostatic repulsion. Certainly, MSN-HAgel was apt to aggregate near pH 6.0 because its zeta potentials were near zero. Inset TEM images of MSN-HA and MSN-HAgel at pH
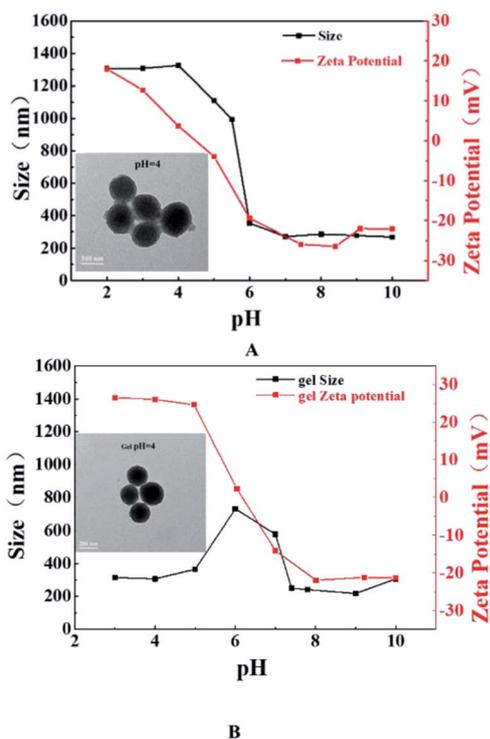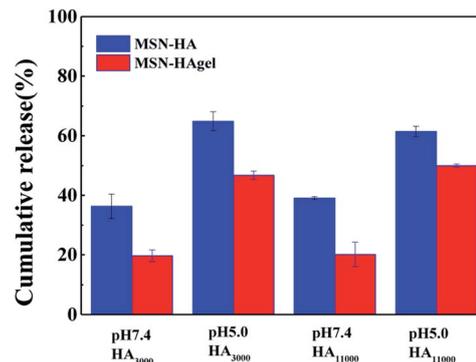


Fig. 3 Simulated release of uncrosslinked MSN-HA@DOX and crosslinked MSN-HAgel @DOX after 48 h.

= 4.0 could also be illustrated. Further, according to the results shown in Fig. 4, the triggering pHs of MSN-HA and MSN-HAgel were considered to be near 6.0.

**3.2.2 The drug blocking effect.** The drug blocking effects of MSN-HA and MSN-HAgel are shown in Fig. 3. As to MSN-HA$_{3000}$gel, the final drug release rate after HA crosslinking reduced from 36.3% to 19.7% under pH 7.4 and reduced from 64.9% to 46.7% at pH 5.0. It could be easy to understand that the HA crosslinking increased drug encapsulation effect, inducing a less drug leakage especially under normal physiological conditions. Meanwhile, the drug leakage of MSN-HA at pH 7.4 was found to be smaller than that at pH 5.0, which was considered to result from the better permeability under the pH 5.0 condition.

### 3.3. Effect of molecular weight of HA on *in vitro* DOX release of MSN-HAgel

Here, HA with molecular weights of 3000 g mol$^{-1}$ and 11 000 g mol$^{-1}$ were selected. First, DOX was tried to be loaded into MSN-HAgel under different pHs and their values of DEE and DLC are listed in Table S2†. It could be found that the average DEE and DLC of MSN-HA$_{3000}$gel in PBS with pH 8.5 were 71.6% and 6.7% respectively, while those were only 33% and 2% under neutral conditions. The isoelectric point of DOX was near pH 8.5 and it was almost neutral under pH 8.5, and the electrostatic interaction between DOX and HA was weakened, making it easier for the drug to go through HA into the MSN and resulting in higher DOX loading efficiency. Thus, the drug was encapsulated in an alkaline PBS buffer with pH 8.5 in later experiments. Moreover, it was also found that the size of the HA chain showed no direct relevance to DEE and DLC values, indicating that HA with a molecular weight of 3000 g mol$^{-1}$ was long enough to block drugs.

The DOX release curves of MSN-HA$_{3000}$gel and MSN-HA$_{11000}$gel are shown in Fig. 4 for discussing the effect of HA size. As shown in Fig. 4A-1, under pH 7.4 and GSH-free condition, the DOX release lines became plateaued after 8 h, and the release rate after 48 h was about 20%. It could be thought that the drug carrier had perfect drug encapsulation with low leakage. Next, under the conditions of pH 7.4 and GSH, the
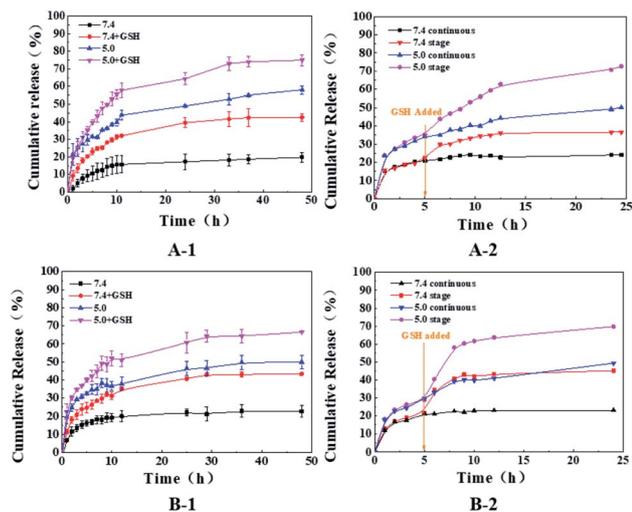


Fig. 2 Particle size and zeta potential of MSN-HA (A) and MSN-HA$_{3000}$gel (B) at different pHs ($c = 0.1$ mg mL$^{-1}$). Inset: TEM images under pH 4.0 (scale bar: 200 nm).

**Fig. 4** *In vitro* DOX cumulative release and stage release of MSN-HA$_{3000}$ (A) and MSN-HA$_{11000}$gel (B).



**Fig. 5** *In vitro* HApt release of MSN-HA$_{3000}$gel.

crosslinking bridge S–S collapsed and HAgel became a loose "brush" structure. The drug was released rapidly and the release rate reached about 51.5% after 48 h. Furthermore, under the condition of pH 5.0, the release rates increased significantly to 56% without GSH and 74% with GSH. According to the above zeta potential study, the isoelectric point of MSN-HAgel was pH 6.0 and then the repulsive interaction between the HA chains made the HA layer have higher permeability.

As compared in Fig. 4A-1 and B-1, the release trend of MSN-HA$_{11000}$gel was basically the same as that of MSN-HA$_{3000}$gel. The very similar release rate under pH 7.4 for the two carriers indicated that longer HA chains did not show a better effect on reducing drug leakage under a normal body environment. However, under the combined influence of pH 5.0 and GSH, the final release rate of MSN-HA$_{3000}$gel was higher than that of MSN-HA$_{11000}$gel, which was considered relevant to a thick HA layer when using a longer HA.

Furthermore, stage drug release behaviors of the two carriers under different pH values are shown in Fig. 4A-2 and B-2, respectively. Continuous releases were that GSH was not added, while stage releases were that GSH was added after 5 h. With the addition of GSH, the drug release rate in both Fig. 4A-1 and B-1 increased sharply, while groups without GSH tended to be flat. It could be seen that both MSN-HA$_{3000}$gel and MSN-HA$_{11000}$gel had good GSH responses.

### 3.4. *In vitro* HApt release of MSN-HA$_{3000}$gel

Texas red-HApt-SH was added and grafted onto HA *via* an S–S bond when HA gel formed and its standard curve of fluorescence is listed in Fig. S3†. As shown in Fig. 5, the release of HApt was slow and the final release was less than 20% without GSH. This part of HApt was thought to be encapsulated in the HA gel layer, and not connected to HA by an S–S bond. However, under the action of GSH, HApt fell from the hyaluronic acid chain rapidly in the first 6 h, and the final release amount could reach above 60%. There were no significant differences in the release
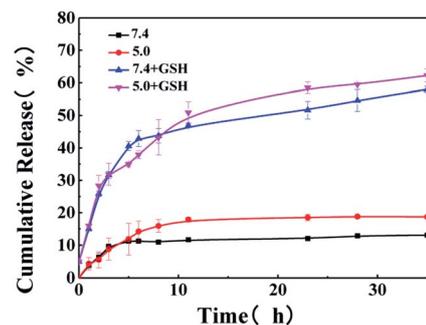
trend of HApt under the conditions of pH 5.0 and pH 7.4. The release of HApt of pH 5.0 was slightly higher than that of pH 7.4, which might be due to the less effect between HA and HApt under acidic conditions. Although the HApt nucleic acid molecules were detached from the carrier under the action of GSH at pH 7.4, since the nucleic acid molecules were negatively charged and the carrier was positively charged at this time, there was still a small amount of HApt molecules that were not fully released due to electrostatic action, while the HApt molecule was positively charged and had electrostatic repulsion with the carrier under acidic conditions.

### 3.5. Biocompatibility and cytotoxicity experiments

SKBR3 cancer cells overexpressing HER2 receptors and HepG2 cancer cells without HER2 receptors were selected in cell experiments. The *p*-values were calculated using SPSS data analysis software and *p*-values <0.05(*) were considered to be significant. Biocompatibility of MSN-HA and MSN-HAgel is shown in Fig. 6A and B, respectively. Evidently, compared to the control group ($c = 0$ μg mL$^{-1}$), both MSN-HA and MSN-HAgel had good biocompatibility to HepG2 cells when the carrier
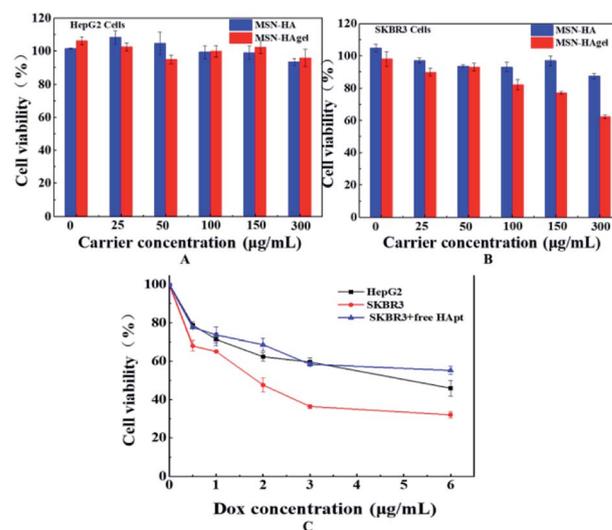


**Fig. 6** Biocompatibility of MSN-HA and MSN-HAgel to HepG2 cells (A) and SKBR3 cells (B); (C) cytotoxicity of MSN-HAgel@DOX to different cells.

concentrations were less than 150 μg mL$^{-1}$ ($p > 0.05$). Even when the carrier concentration reached 300 μg mL$^{-1}$, although significant cytotoxicity was observed ($p < 0.01$), the cell viability was still above 90%, suggesting that HApt could not work without HER2 receptors. As to SKBR3 cells, MSN-HA still showed good biocompatibility. However, MSN-HAgel showed evident cytotoxicity when its concentration was above 100 μg mL$^{-1}$ ($p < 0.01$), and the cell death rate was 30% at 300 μg mL$^{-1}$, indicating that HApt on MSN-HAgel could enter the cell effectively through endocytosis and then induce apoptosis.

Fig. 6C shows the cytotoxicity of MSN-HAgel@DOX to the two cells. The blue line was the cytotoxicity to the SKBR3 cells whose HER2 receptor had been shielded by pre-incubation with free HApt for 30 min, which showed similar cytotoxicity to those of HepG2 cells. Also, it was found that the toxicity of MSN-HAgel@DOX to SKBR3 cells was stronger than that to HepG2, indicating that the combination of HApt and HER2 receptor was efficient.

The SKBR3 groups with a DOX concentration of 6 μg mL$^{-1}$ were selected for comparison. Compared to the blank group (MSN-HA), all the groups showed significant cytotoxicity to SKBR3 cells ($p < 0.01$). As shown in Fig. 7, the blank carrier MSN-HA without DOX and HApt had a cell viability near 100%, while that of HApt-contained MSN-HAgel was 80%, which indicated that although the HApt was hidden in HAgel, it still maintained enough bioactive function after being clipped down by GSH. As to the toxicity of DOX, whether it was free or loaded in MSN-HA (without HApt), it had a cell viability of about 75%. Further, when the sample contained both HApt and DOX (MSN-HAgel@DOX), its cell viability decreased sharply to only 35%, showing a "1 + 1 > 2" synergistic therapeutic effect, which verified that the HApt hidden in HAgel could recognize HER2 protein on the cell membrane. The HApt molecule could target the lysosome of SKBR3, and its toxic effect depended on the activity of the lysosome, which mainly induced apoptosis by degrading HER2 in the lysosome. Meanwhile, the targeted recognition of HApt to HER2 receptor allowed the carriers to enter the cell and increase the drug effect, and this synergistic effect of gene and chemotherapeutics had been previously studied by our group.[19,43] This enhanced synergistic treatment effect has been studied by more researchers, which is beneficial to solve the limitations of single treatment or multidrug resistence.[44,45]

## 4. Conclusion

In this study, two types of oligomeric HA were grafted to the surface of MSN. Then, the modified HA was crosslinked through disulfide bonds for better DOX encapsulation. At the same time of crosslinking, the small DNA molecule HApt was introduced for providing targeting ability to HER2 receptors. The DOX release of MSN-HAgel was less than 20% under the normal body fluid environment while realized rapid release in the tumor microenvironment. The in vitro simulated release of DOX showed good pH/reduction dual stimulus response performance. And the release of the HApt was found to show great response to GSH as expected. The difference in molecular weight of the two oligomeric HA had little effect on the drug release and physical properties. The usage of HA$_{3000}$ was able to achieve drug encapsulation and an excessively long HA chain might lead to difficult drug release. As shown in cell experiments, MSN-HA exhibited good biocompatibility even when the carrier concentration reached 300 μg mL$^{-1}$. The cytotoxicity test showed that HApt molecules had a great targeting effect and cytotoxicity to SKBR3 overexpressing HER2 receptor on the cell surface. It has been confirmed that the MSN-HAgel could transport gene and chemical drugs into the cell simultaneously and realized the synergistic effect of "1 + 1 > 2". In summary, a drug-loaded nanocarrier that could not only achieve pH/reduction dual stimulation response but also efficiently combine drug and gene therapy was constructed. This study provided a new idea for clinical tumor treatment, which had good application potential.

## Conflicts of interest

The authors declare that they have no known competing financial interests or personal relationships that could have appeared to influence the work reported in this paper.

## Acknowledgements

## References

1 F. Bray, et al., Global cancer statistics 2018: GLOBOCAN estimates of incidence and mortality worldwide for 36 cancers in 185 countries, Ca-Cancer J. Clin., 2018, **68**(6), 394–424.

2 S. Huang and G. Huang, Preparation and drug delivery of dextran-drug complex, Drug Delivery, 2019, **26**(1), 252–261.
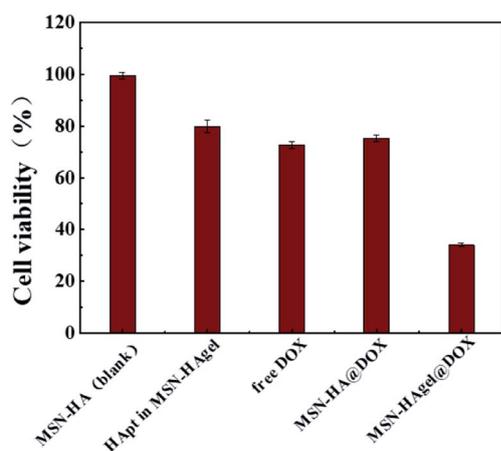
**Fig. 7** Studies of synergistic therapeutic effects to SKBR3 cells (concentration of MSN-HA and MSN-HAgel: 150 μg mL$^{-1}$, DOX concentration of other samples: 6 μg mL$^{-1}$).

3  M. Vallet-Regi, *et al.*, A New Property of MCM-41: Drug Delivery System, *Chem. Mater.*, 2001, **13**(2), 308–311.

4  H. R. Mellor and R. Callaghan, Resistance to Chemotherapy in Cancer: A Complex and Integrated Cellular Response, *Pharmacology*, 2008, **81**(4), 275–300.

5  M. Nelson-Veniard and J.-B. Thambo, Cardiotoxicité des chimiothérapies chez l'enfant : type, dépistage et prévention, *Bull. Cancer*, 2015, **102**(7), 622–626.

6  B. Zhou, *et al.*, Immunologically modified $MnFe_2O_4$ nanoparticles to synergize photothermal therapy and immunotherapy for cancer treatment, *Chem. Eng. J.*, 2020, **396**, 125239.

7  Z. Li, *et al.*, A pH-responsive polymer linked with immunomodulatory drugs: synthesis, characteristics and in vitro biocompatibility, *J. Appl. Toxicol.*, 2021, **41**(5), 724–735.

8  S. Heinävaara and T. Hakulinen, Predicting the lung cancer burden: accounting for selection of the patients with respect to general population mortality, *Stat. Med.*, 2006, **25**(17), 2967–2980.

9  V. Biju, Chemical modifications and bioconjugate reactions of nanomaterials for sensing, imaging, drug delivery and therapy, *Chem. Soc. Rev.*, 2014, **43**(3), 744–764.

10  Z. Li, N. Song and Y.-W. Yang, Stimuli-Responsive Drug-Delivery Systems Based on Supramolecular Nanovalves, *Matter*, 2019, **1**(2), 345–368.

11  T. M. Allen and P. R. Cullis, Liposomal drug delivery systems: From concept to clinical applications, *Adv. Drug Delivery Rev.*, 2013, **65**(1), 36–48.

12  B. Lei, *et al.*, Double security drug delivery system DDS constructed by multi-responsive (pH/redox/US) microgel, *Colloids Surf., B*, 2020, **193**, 111022.

13  Z. Luo, *et al.*, Mesoporous Silica Nanoparticles End-Capped with Collagen: Redox-Responsive Nanoreservoirs for Targeted Drug Delivery, *Angew. Chem., Int. Ed.*, 2011, **50**(3), 640–643.

14  H. Maeda and Y. Matsumura, EPR effect based drug design and clinical outlook for enhanced cancer chemotherapy, *Adv. Drug Delivery Rev.*, 2011, **63**(3), 129–130.

15  M. Yu, *et al.*, Hyaluronic acid modified mesoporous silica nanoparticles for targeted drug delivery to CD44-overexpressing cancer cells, *Nanoscale*, 2013, **5**(1), 178–183.

16  W. Wang, *et al.*, Biomineralization: An Opportunity and Challenge of Nanoparticle Drug Delivery Systems for Cancer Therapy, *Advanced Healthcare Materials*, 2020, **9**(22), 2001117.

17  Y. Yu, *et al.*, Well-Defined Degradable Brush Polymer–Drug Conjugates for Sustained Delivery of Paclitaxel, *Mol. Pharm.*, 2013, **10**(3), 867–874.

18  J. Kecht, A. Schlossbauer and T. Bein, Selective Functionalization of the Outer and Inner Surfaces in Mesoporous Silica Nanoparticles, *Chem. Mater.*, 2008, **20**(23), 7207–7214.

19  Y. Shen, *et al.*, A dual-functional HER2 aptamer-conjugated, pH-activated mesoporous silica nanocarrier-based drug delivery system provides in vitro synergistic cytotoxicity in HER2-positive breast cancer cells, *Int. J. Nanomed.*, 2019, **14**, 4029–4044.

20  J. Xu, *et al.*, A dual-responsive drug delivery system based on mesoporous silica nanoparticles covered with zipper-type peptide for intracellular transport/release, *Colloids Surf., A*, 2021, **631**, 127672.

21  J. Li, *et al.*, Biospecific Self-Assembly of a Nanoparticle Coating for Targeted and Stimuli-Responsive Drug Delivery, *Adv. Funct. Mater.*, 2015, **25**(9), 1404–1417.

22  E. Aznar, *et al.*, Gated Materials for On-Command Release of Guest Molecules, *Chem. Rev.*, 2016, **116**(2), 561–718.

23  N. Ž. Knežević and V. S. Y. Lin, A magnetic mesoporous silica nanoparticle-based drug delivery system for photosensitive cooperative treatment of cancer with a mesopore-capping agent and mesopore-loaded drug, *Nanoscale*, 2013, **5**(4), 1544–1551.

24  H. Meng, *et al.*, Correction to Use of a Lipid-Coated Mesoporous Silica Nanoparticle Platform for Synergistic Gemcitabine and Paclitaxel Delivery to Human Pancreatic Cancer in Mice, *ACS Nano*, 2016, **10**(6), 6416.

25  E. Aznar, *et al.*, Glucose-triggered release using enzyme-gated mesoporous silica nanoparticles, *Chem. Commun.*, 2013, **49**(57), 6391–6393.

26  R. Thapar, *et al.*, RNA Modifications: Reversal Mechanisms and Cancer, *Biochemistry*, 2019, **58**(5), 312–329.

27  F. Zamboni, *et al.*, Labile crosslinked hyaluronic acid via urethane formation using bis(β-isocyanatoethyl) disulphide with tuneable physicochemical and immunomodulatory properties, *Carbohydr. Polym.*, 2020, **245**, 116501.

28  T. Walimbe, A. Panitch and P. M. Sivasankar, A Review of Hyaluronic Acid and Hyaluronic Acid-based Hydrogels for Vocal Fold Tissue Engineering, *J. Voice*, 2017, **31**(4), 416–423.

29  Q. Zhao, *et al.*, Dual-stimuli responsive hyaluronic acid-conjugated mesoporous silica for targeted delivery to CD44-overexpressing cancer cells, *Acta Biomater.*, 2015, **23**, 147–156.

30  J. Couzin-Frankel, Autoimmune diseases surface after cancer treatment, *Science*, 2017, **358**(6365), 852.

31  W. Wang, *et al.*, Nanoscale Polymer Metal–Organic Framework Hybrids for Effective Photothermal Therapy of Colon Cancers, *Adv. Mater.*, 2016, **28**(42), 9320–9325.

32  S. Xu and M. Yonese, Two Dimensional and Three Dimensional Interactions between Bovine Serum Albumin and Chondroitin Sulfate, *Polym. J.*, 2007, **39**(4), 298–303.

33  S. H. Xu, *et al.*, Characteristics of complexes composed of sodium hyaluronate and bovine serum albumin, *Chem. Pharm. Bull.*, 2000, **48**(6), 779–783.

34  S. Ghosh, *et al.*, Targeted delivery of curcumin in breast cancer cells via hyaluronic acid modified mesoporous silica nanoparticle to enhance anticancer efficiency, *Colloids Surf., B*, 2021, **197**, 111404.

35  J. Zhang, *et al.*, Multifunctional mesoporous silica nanoparticles modified with tumor-shedable hyaluronic acid as carriers for doxorubicin, *Colloids Surf., B*, 2016, **144**, 293–302.

36  S. L. Ginn, *et al.*, Gene therapy clinical trials worldwide to 2012 – an update, *J. Gene Med.*, 2013, **15**(2), 65–77.

37 A. Morgan Richard, *et al.*, Cancer Regression in Patients After Transfer of Genetically Engineered Lymphocytes, *Science*, 2006, **314**(5796), 126–129.

38 P. F. Robbins, *et al.*, Tumor Regression in Patients With Metastatic Synovial Cell Sarcoma and Melanoma Using Genetically Engineered Lymphocytes Reactive With NY-ESO-1, *J. Clin. Oncol.*, 2011, **29**(7), 917–924.

39 R. Vivek, *et al.*, Multifunctional HER2-Antibody Conjugated Polymeric Nanocarrier-Based Drug Delivery System for Multi-Drug-Resistant Breast Cancer Therapy, *ACS Appl. Mater. Interfaces*, 2014, **6**(9), 6469–6480.

40 P. N. Munster, *et al.*, Degradation of HER2 by ansamycins induces growth arrest and apoptosis in cells with HER2 overexpression via a HER3, phosphatidylinositol 3′-kinase-AKT-dependent pathway, *Cancer Res.*, 2002, **62**(11), 3132–3137.

41 H. Roh, J. Pippin and J. A. Drebin, Down-regulation of HER2/neu expression induces apoptosis in human cancer cells that overexpress HER2/neu, *Cancer Res.*, 2000, **60**(3), 560–565.

42 G. Mahlknecht, *et al.*, Aptamer to ErbB-2/HER2 enhances degradation of the target and inhibits tumorigenic growth, *Proc. Natl. Acad. Sci. U. S. A.*, 2013, **110**(20), 8170–8175.

43 Y. Shen, *et al.*, Copolymer micelles function as pH-responsive nanocarriers to enhance the cytotoxicity of a HER2 aptamer in HER2-positive breast cancer cells, *Int. J. Nanomed.*, 2018, **13**, 537–553.

44 Z. Fan, *et al.*, Reversing cold tumors to hot: An immunoadjuvant-functionalized metal-organic framework for multimodal imaging-guided synergistic photo-immunotherapy, *Bioact. Mater.*, 2021, **6**(2), 312–325.

45 S. Gao, *et al.*, Selenium-Containing Nanoparticles Combine the NK Cells Mediated Immunotherapy with Radiotherapy and Chemotherapy, *Adv. Mater.*, 2020, **32**(12), 1907568.